AN INITIAL RESOURCE ASSESSMENT OF THE MENENGAI CALDERA GEOTHERMAL SYSTEM USING AN AIR-WATER TOUGH2 MODEL

Ezekiel Kipyego[1], John O'Sullivan[2] and Mike O'Sullivan[2]

[1]Geothermal Development Company, Nairobi, Kenya

[2]Department of Engineering Science, University of Auckland, Private Bag 92019, Auckland 1142, New Zealand

KIPYEGO_ezekiel.kipyego@gmail.com

Keywords: *Geothermal Reservoir Model, Menengai, Kenya, TOUGH2.*

ABSTRACT

The Menengai geothermal field in Kenya is hosted in a ring-like caldera of approximately 12 km diameter. A three-dimensional numerical model of the system has been developed based on a conceptual model derived from the available surface exploration and field data. The model was developed using AUTOUGH2 with the air-water equation-of-state EOS3 allowing the shallow unsaturated zone to be included. The model domain covers an area of 432 km^2 with higher resolution in the upflow regions and extends to a depth of 3200 m where supercritical conditions are known to begin.

Natural state modelling was carried out and good agreement with downhole temperatures has been achieved. The position of the unsaturated zone is represented well, including the position of surface outflows. The explicit inclusion of caldera structures was found to be necessary in order to match the strongly differing downhole temperature profiles of neighbouring wells. The model also predicts the formation of steam zones at the correct elevations.

Production history matching simulations were performed using a limited amount of field data and the model results agree well with measured discharge enthalpies. The model was then used to estimate the performance of the reservoir under a number of possible production regimes. These included targeting feedzones at different depths and testing various reinjection strategies. The results of these scenarios are presented.

1. INTRODUCTION

In 2010, the Menengai geothermal field became the second geothermal field in Kenya to be investigated for development, following on from the Olkaria geothermal project which has proved to be commercially successful. The Menengai geothermal field is located in the Eastern branch of the Gregory Rift Valley (Figure 1) approximately 100 km from the Olkaria field and is hosted in a ring-like caldera of approximately 8 km diameter. The Kenyan rift has significant geographical and geological importance due in part to its volcano-tectonic features and their associated hydrothermal activity which are thought to host a number of viable geothermal systems, as shown in Figure 1. The field is hosted in the Menengai caldera, described as a major topographical feature of the rift valley and the best preserved Krakatau-style caldera in the world (Leat, 1984).

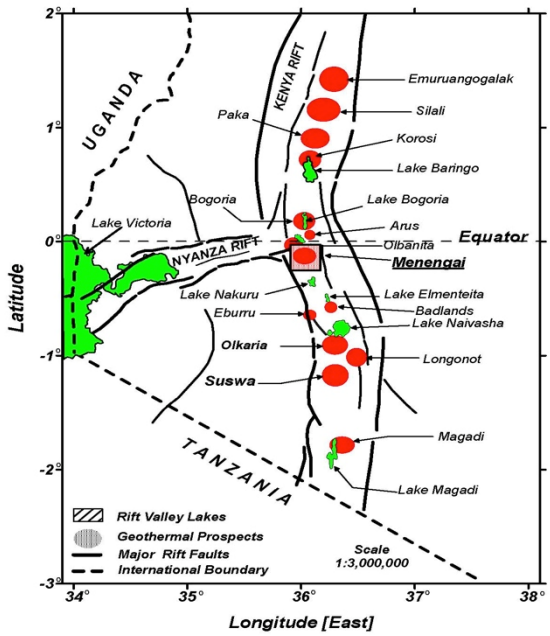

Figure 1: Location of the Menengai geothermal field at the Triple junction. Other geothermal sites are also indicated. Adapted from Simiyu (2009).

Surface exploration has been carried since 2004 and the most promising region at the centre of the Menengai caldera was selected for exploration drilling. Since 2011, several exploration wells have been drilled within the caldera and a maximum temperature of 392^{o}C has been measured in some wells demonstrating the potential of the field for energy production.

In this study, a conceptual model of the Menengai system was developed using information collected from a range of geological, geochemical and geophysical sources. The conceptual model was then used to develop a natural state numerical model which was calibrated using downhole temperatures and water table information. A preliminary assessment of the production capacity of the reservoir was undertaken by applying a number of possible development scenarios. The simulations were carried out using the AUTOUGH2 computer code (Yeh *et al.*, 2012), the University of Auckland version of TOUGH2 (Pruess *et al.*, 1999) and in all cases the equation of state was used for a mixture of air, water and steam (EOS3).

2. CONCEPTUAL MODEL OF THE MENENGAI GEOTHERMAL FIELD

Before a computer model of a geothermal field can be set up, a conceptual model must be developed. The conceptual model summarizes the overall understanding of the important physical and chemical processes that control the reservoir. It is usually represented by two or three sketches showing a plan view and vertical sections of the geothermal system (O'Sullivan *et al*., 2001). The sketches contain the most important characteristics, such as surface manifestations (i.e. hot springs, steaming grounds, etc.), flow boundaries, the main geologic features such as faults and layers, zones of high and low permeability, isotherms, location of deep inflows and boiling zones, geophysical data (resistivity boundaries, heat flow contours). In the following sections, the key information from various sources is discussed before the conceptual model is presented.

2.1 Surface geology

The geology of the Menengai area has been studied and described at several different levels (Jones & Lippard, 1979; Leat, 1984). The surface geology of Menengai is largely composed of late Quaternary volcanics. The caldera floor is covered by pyroclastics and lava flows, while the country around the caldera has air-fall pumice (Leat, 1984). The area north of Menengai is characterized by lavas of trachytic and trachy-phonolitic composition, associated with north-south (N-S) trending fissures (Lagat *et al*., 2010). The lavas underlie the Menengai ignimbrites, Olbanita volcanics and Olrongai volcanics. Pre-caldera Menengai shield trachytes and Menengai tuffs occur south and around the caldera rim areas (Omondi, 2011). Basaltic lavas dominate the Solai axis, Olbanita and Olrongai areas, which are low-lying, are covered with thick soils derived mainly from pyroclastics and extensive thick ignimbrite beds from the caldera.

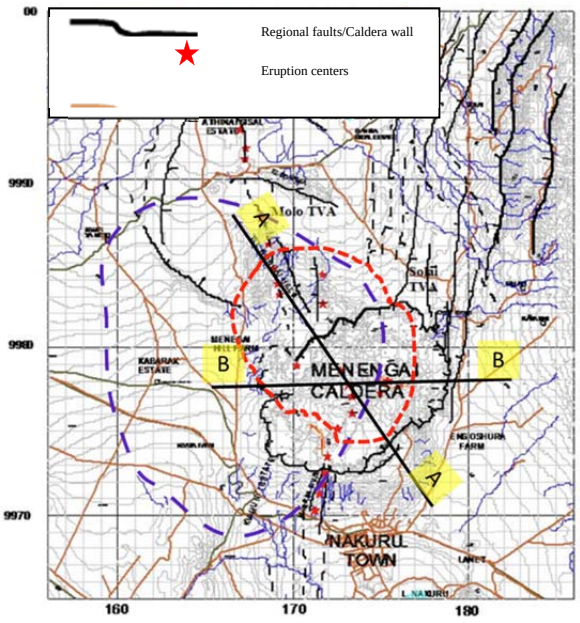

Figure 2: Map of the Menengai geothermal field showing the structural geology, anomalous region with resistivity less than 40Ω (dotted red line) and region associated with hot/warm water (dotted purple line).

The association of many geothermal systems to volcanics of recent origin, especially those characterized by the eruption of acidic magma, means that Menengai is likely to be a good geothermal resource.

2.2 Subsurface geology

The borehole geology indicates that the subsurface stratigraphic structure of the Menengai caldera consists of three main rock units, inherited from the evolution history of the caldera. The rocks are described as pre-caldera, syn-caldera and post-caldera volcanics. The post- and syn-caldera rocks occur from the surface down to ~1600 masl, where the syn-caldera volcanics form a transition layer, of thickness of about 100m, above the pre-caldera rocks. The deeper pre-caldera rocks are predominantly trachytic with tuffaceous intercalations at various elevations, including 1300-1400, 400-600, and 100-200 masl.

2.3 Structural geology

The main structural features in the field are the Menengai caldera, the Molo TVA, the Solai graben (Kipng'ok, 2011) and the Olbanita buried caldera (Riaroh & Okoth, 1994). Structurally the Menengai caldera is complex. In the northeast corner of Menengai caldera the caldera wall is cut by the N-S trending Solai graben which is parallel to the group of N-S trending faults northeast of Menengai (Figure 2). Within the caldera there are numerous smaller faults trending both northeast-southwest (NE-SW) and northwest-southeast (NW-SE) (Mibei, 2011).

2.4 Exploration Drilling

At the time of this study, 13 exploration wells had been drilled in the Menengai geothermal field mainly towards the centre of the caldera. According to geophysical resistivity and seismic surveys, this area is likely to be the most productive (Lagat *et al*., 2010; Simiyu, 2009). However, the resistivity information shows that the geothermal reservoir also extends from the centre of the caldera towards the northwest as far as the Olrongai ridge (Figure 2). The wells have been drilled to average depths of between 2000 and 2300m. Data from well tests was available for this study from only six of the 13 wells and Table 1 summarizes the specifications of the wells considered.

Table 1: Specifications of six exploration wells.

Well	MW01	MW03	MW04	MW06	MW08	MW09
Well-head						
Easting (m)	171847	173993	173311	172853	173237	172848
Northing (m)	9976849	9977009	9977517	9976761	9978210	9977301
Elevation	2054	2064	2098	2102	2018	2105
Drilled depth	2198	2106	2118	2181	2338	2088
Permeable zones (masl)	854 - 654 454 - 304 154 - 46	1300 - 1100	298 - 398	300 - 100	1000 - 900	800 - 200
Maximum temperature (°C)	391	332	392	325	325	306

2.5 Conceptual model design

An upflow of high temperature fluid (above 300°C) arises beneath the Menengai caldera through buried structures and is manifested at the surface by fumaroles. The geochemical analysis of the fumarolic gas indicates a deep, high temperature reservoir. Two separate boiling zones at elevations between 1000 to 1500 masl and 400 to 700 masl were identified from hydrothermal alteration of minerals occurring there.

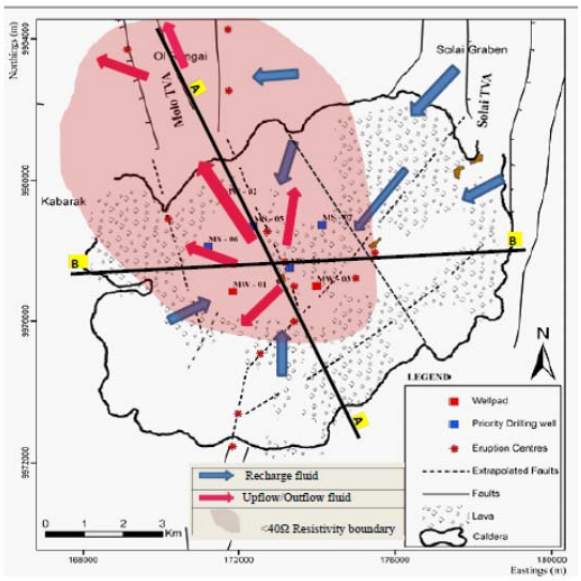

Figure 3: Fluid flow in Menengai geothermal field.

Temperature contours drawn using the measured data from the exploration wells suggest an increasing trend towards the centre of the caldera which indicates a likely upflow zone of high temperature fluid. The heat source for the system is a shallow magma chamber with a hot intrusive penetrating into the reservoir (Lagat, 2011).

Recharge of cold water is from the east and northeast of the geothermal field. Local and regional recharge into the reservoir is controlled by major faults trending NW-SE along the minor axis of the caldera (Leat, 1984), the caldera wall and other minor structures in the caldera. Both complex subsurface fractures and lithologic contacts provide the permeability controlling recharge and upflow.

There is a probable fluid flow in the NW, West and NE directions from the upflow region, forming the outflow of the Menengai reservoir, (Figures 3 and 4). The outflow areas were inferred by the presence of warm to hot shallow boreholes in these regions (McCall, 1967; Wheildon *et al*., 1994).

The plan view and cross-section B-B of the conceptual model are presented in Figures 3 and 4 respectively.

3. MENENGAI RESERVOIR MODEL

The numerical model developed in this work was based on the conceptual model described above. An air/water model was used and the simulations carried out using the AUTOUGH2 code.

3.1 Model extent, location and grid structure

The Menengai geothermal system was modelled using a rectangular prism 24 km long by 18 km wide and 3 km deep. The model was positioned so that the entire caldera was covered, with at least a 2 km buffer between the caldera wall and the edge of the model. It was also considered large enough to capture the meteoric recharge for the system. In the north, the domain was extended so that the model covered the Olrongai ridge and the Barina swamp where the water table reaches the surface.

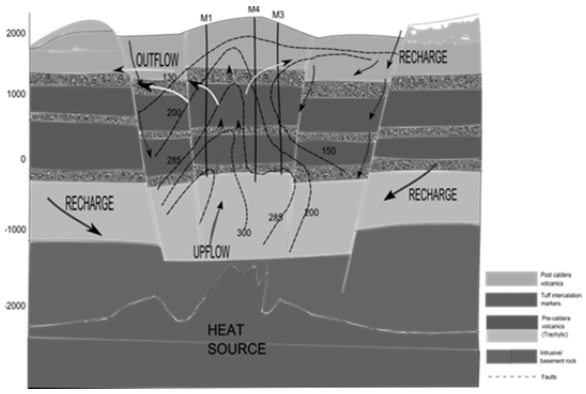

Figure 4: E-W cross section through the Menengai caldera (Section B-B in Figure 2).

The depth of the model was determined using downhole temperatures and also taking account of the maximum temperature of 370^{o}C that can be simulated with the standard AUTOUGH2 code.

The grid system consists of 8391 blocks in 17 vertical layers, numbered from top to bottom. Some blocks in the top layers have been omitted, while the thickness of others has been reduced to set up a grid that follows the topography. The layer thickness ranges from 100 m to 500 m and the model extends from an elevation of 2200 masl to -1000 masl. At the edges of the model, the grid blocks are 2km by 2km but two levels of local refinement were used to create a higher resolution grid in the areas of most interest. The exploration drilling area is represented by smaller grid blocks (250 m by 250 m) within an area of 3.5 km by 3.5 km as shown in Figure 5.

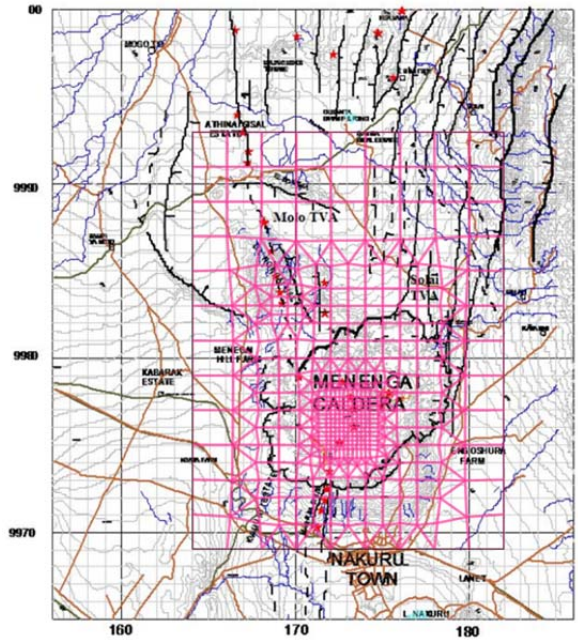

Figure 5: Model grid design overlaid on a map of the Menengai caldera and the surrounding area.

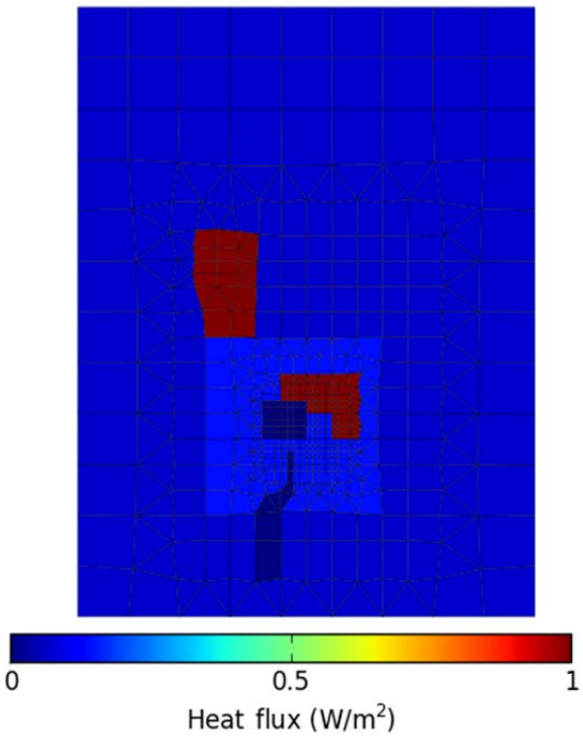

Figure 6: Heat flux boundary condition at the bottom of the model.

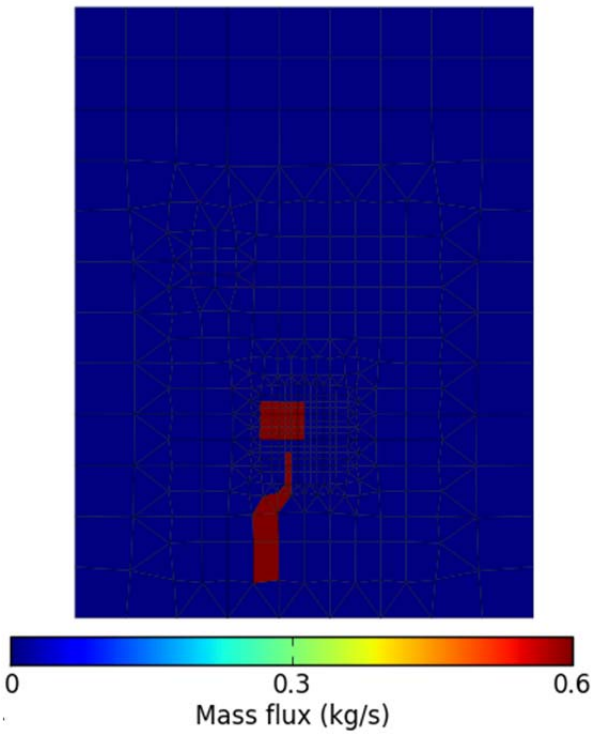

Figure 7: Mass flux boundary condition at the bottom of the model.

3.2 Boundary conditions

At the top surface of the model, the atmospheric layer was set to contain air at standard atmospheric pressure and a constant temperature of 20°C. The infiltration of rainwater at the surface was approximated by the injection of 20°C water with an enthalpy of 83.9 kJ/kg into the top layer of the model. The injection rate of 1.0E-6 kg/m^{2}s was used which corresponds to an annual average rainfall of 1050 mm/yr with an infiltration rate of 3%. Also, water at 20°C is injected into the surface block corresponding to the point where the Bahati stream enters the caldera and disappears into the subsurface. An estimated flow rate of 100 l/s is used to represent the stream.

The lateral boundaries of the model to the south, east and west were set to be closed thus enforcing no flow across them. This is an approximation of the real system and is the motivation for placing the model boundaries as far from the reservoir as computational cost will allow (O'Sullivan *et al*., 2001). For the Menengai system, it is clear that ground water flow continues from the areas north of the caldera, north to the Barina swamp and beyond. To take this into account, deliverability wells (Pruess *et al*., 1999) were assigned in the blocks at the northern edge of the model in the layers down to a depth of 300m below the surface. These wells allow groundwater to flow out of the model as required to achieve a hydrostatic pressure gradient at the edge.

As described above, the grid structure was refined in the upflow zones identified by Simiyu (2009) at the Menengai caldera and the Olrongai volcano. In both of these areas additional heat was applied at the bottom boundary of the model, above the background level of 0.07 W/m^2. Figure 6 shows the heat flux distribution at the bottom boundary of the best-fit model with maximum values of 1.05 W/m^2 indicated. The mass flux boundary condition for the same model is shown in Figure 7. Approximately 0.6 kg/s was injected into each of the blocks under the main caldera upflow and those corresponding to the Makalia fault. This input of hot water represents the hot deep upflow that comes from beneath the bottom of the model domain. A high enthalpy of 1670 kJ/kg was used, which corresponds to liquid water at 350°C. This value is less than that recorded at the bottom of the exploration wells but is the maximum that could be used successfully with the standard AUTOUGH2 code. In total, the mass flux at the bottom boundary for the best-fit model was 100 kg/s.

In the real system, it is likely that there is also a significant deep upflow under the Olrongai volcano (Simiyu, 2009). However, at this stage no wells have been drilled in this area making it difficult to calibrate any mass flux assigned to this part of the model. This will be discussed, along with other possible model improvements, in subsequent sections.

3.3 Model geology

The objective of the preliminary model presented in this work was to explicitly represent the major geological formations and structures to a satisfactory level while still maintaining a relatively coarse model. One of simplifying assumptions that was made was that the geological formations were in horizontal layers as determined by the available well geology reports (Omondi, 2011; Mibei, 2011). Seven major composite rock units were defined, as shown in the conceptual model plots. The layer structure of the model is shown in Figure 8 with the rock formations indicated. The model rock-type is also given which determines the first two letters of the five-letter code.

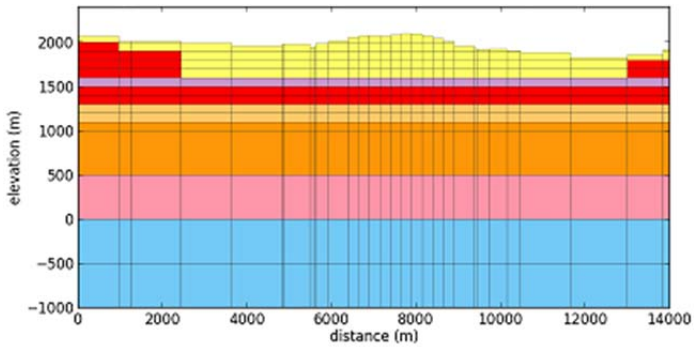

	Rock Type	Model prefix
	Predominantly pyroclastics	TS
	Trachytic tuff	TU
	Trachyte	T0
	Predominantly rhyolite	RH
	Mixture of trachyte and trachy-phonolites	T1
	Predominantly basalt and syenite	BA
	Predominantly trachyte	T2

Figure 8: Vertical rock structure in the model (Section B-B in Figure 2).

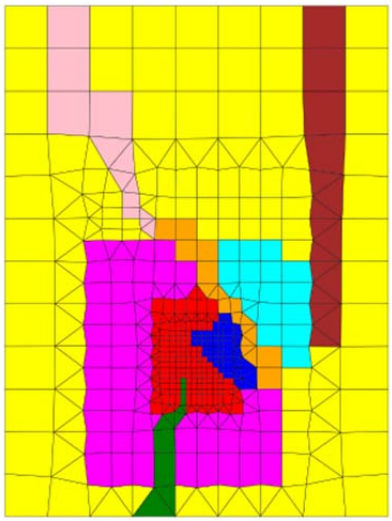

	Structural zone	Model suffix
	Caldera hotter inner zone	CHI
	Caldera colder inner zone	CCI
	Caldera hotter outer zone	CCO
	Caldera colder outer zone	CHO
	Solai TVA	F1
	Molo TVA	F2
	Molo TVA caldera extension	F3
	Makalia fault	F4
	Outer zone	OUT

Figure 9: Horizontal rock structure in the model.

The structures included in the model were the Molo TVA, the Solai TVA, Makalia fault, the caldera wall and an extension of the Molo TVA fault into caldera. The caldera was divided into two along its short axis and then each half was then divided into an inner and outer zone. The dividing line in the caldera roughly separates the exploration wells that are hot in the shallow zone from those that are colder. In each layer, the model rock-type assigned to a given block was based on these structures. The basis for this approach is that the parts of the formation located along a fault or within the caldera may have undergone different stress regimes which have led to different rock properties. Figure 9 shows a plot of the rock-type assignment for a single layer with each structural zone indicated.

In total the vertical and horizontal rock structure combine to give 93 model rock-types and for this preliminary model the following typical values of rock properties were used for all of them:

Porosity	0.1
Rock density	2500 kg/m^3
Thermal conductivity	2.5 W/m^2.^{o}C

3.4 Model calibration

The natural state model was calibrated by iteratively adjusting the permeabilities of each of the model rock-types and the strength and position of the bottom boundary conditions so that the best match with measured downhole temperatures was achieved (O'Sullivan *et al.*, 2001). Measured data for the surface features can also be used to calibrate a model. However, at the time of this study, only qualitative data was available for the surface features and so only qualitative agreement was obtained with the model results. This means that the hottest zones on the surface of the model correspond with the known location of fumaroles and that there are no surface outflows of cold water apart from at the Barina swamp.

4. NATURAL STATE MODEL RESULTS

The results for downhole temperatures produced by the best-fit model are presented in Figure 10. The permeability structure at 1000 masl for the same model is shown in Figure 11 and is discussed in the following section. Plot (b) of Figure 11 shows a detailed view of the locations of the wells and is useful reference for the discussion of the downhole temperatures.

Plot (a) of Figure 10 shows that the model matches the downhole temperatures in MW-01 quite well. The cold inflow in the shallow zone is not present in the model. However, the slight cold inflow at ~250 masl is represented. The high temperatures at the bottom of the well are not predicted due to the limitations of the standard AUTOUGH2 code. This is the case for all of the wells except MW-09. The near-conductive profile of MW-03 is

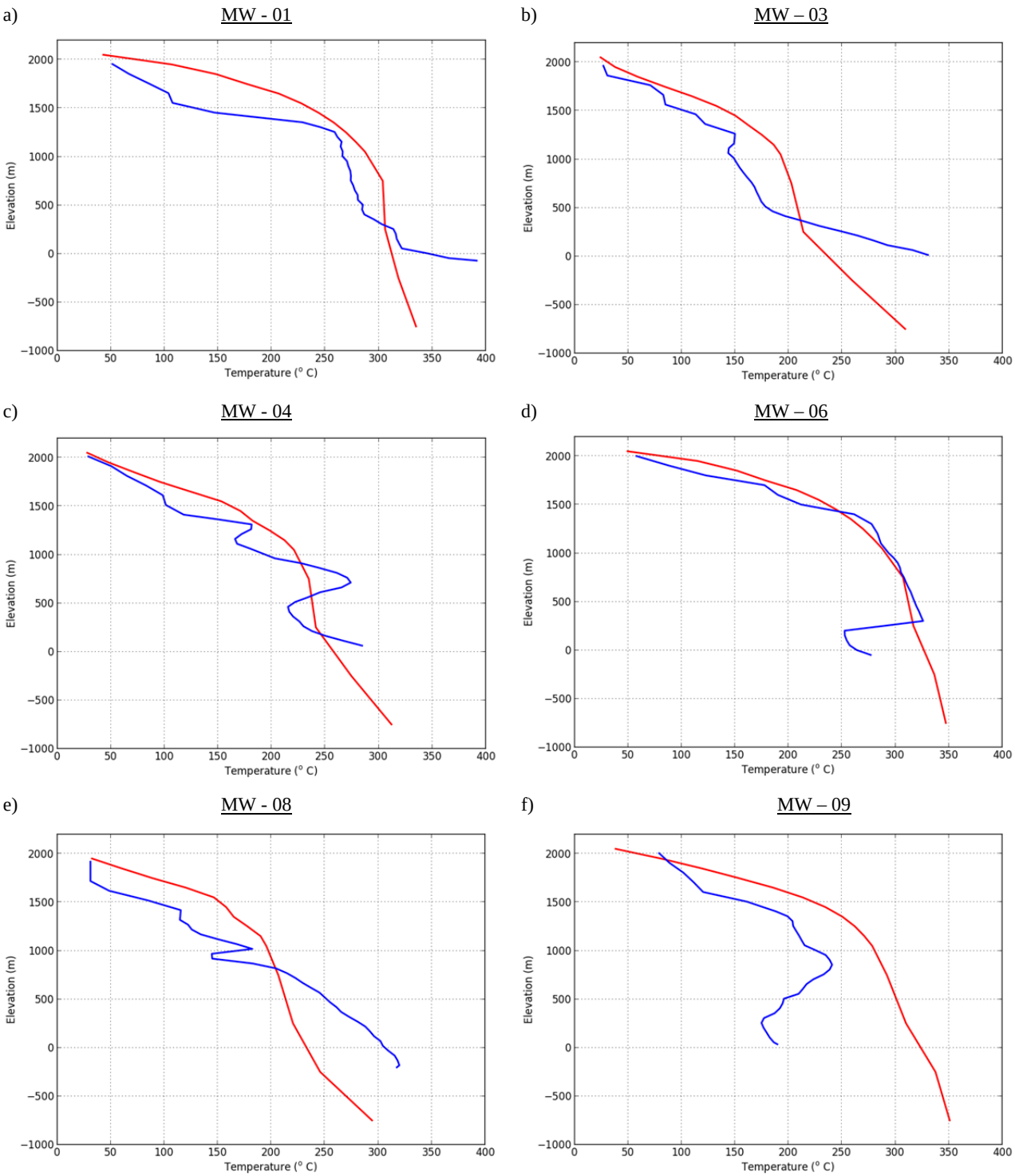

Figure 10: Downhole temperatures for six Menengai exploration wells. Measured data shown in blue and best-fit model results in red.

difficult to represent using a coarse resolution model. Especially given its relatively close proximity to MW-06. However, the model does a good job of matching the small outflow at 1200 masl.

The measured profile for MW-04 also shows it is not in the main upflow and the profile is largely conductive. Unlike MW-03 there are a number of significant inflows and outflows making it difficult to match accurately. Despite this, the model performs quite well in matching the elevations of inflows and outflows though they are not as strong as those observed in the field data. The model estimates the downhole temperatures very well for MW-06 which is in the middle of the upflow zone as shown by the convective profile. The model does not predict the sharp cold inflow at 200 masl, though the accuracy of this field data needs to be confirmed.

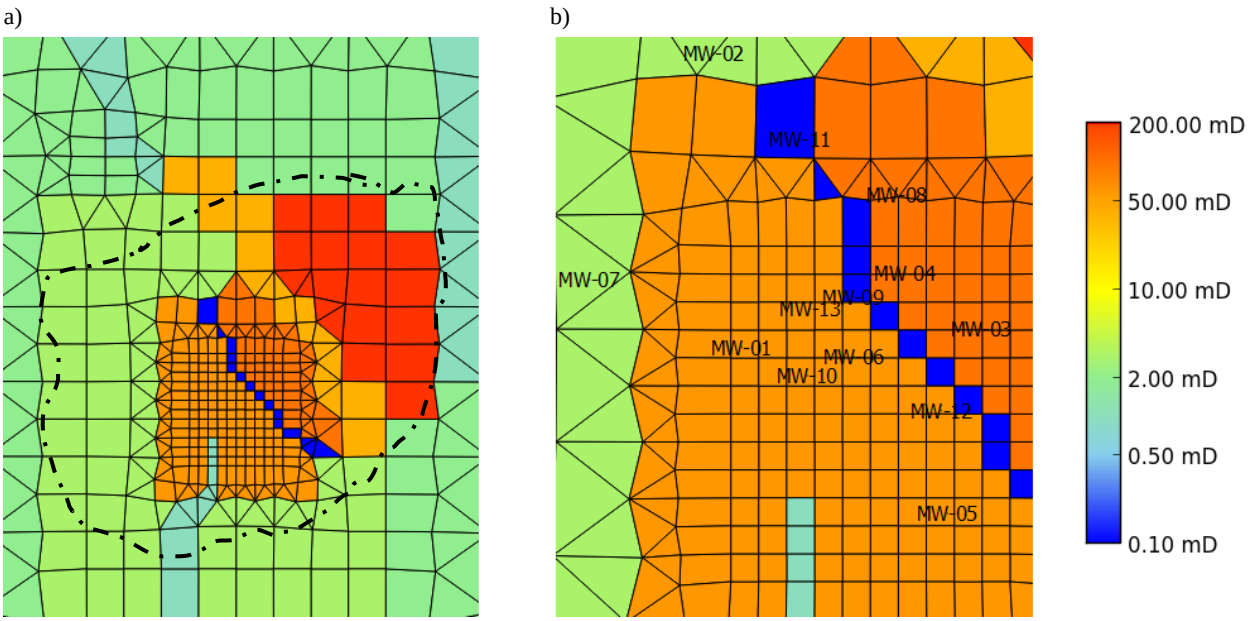

Figure 11: Model horizontal permeability distribution at 1000 masl with the caldera boundary indicated (-.-) in plot (a). The same is shown in plot (b) magnified to show well locations.

Plot (e) in Figure 10 shows that the model also matches the conductive profile measured in MW-08. However, the match for the final well, MW-09, is quite poor. This highlights the limitations of a coarse-resolution model as MW-09 is located close to MW-04, MW-06 and MW-08 but at 200 masl depth, the measured temperature is nearly 100°C less than for the other three wells. The large temperature contrast over a small distance is not matched by the model and an improvement could only be achieved by using a finer grid and more detailed permeability structure.

4.1 Permeability distribution

The permeabilities for model rock-types in the central upflow zone of the caldera in the best-fit natural state model are given in Table 2. The permeability outside the central upflow ranges from 0.5 mD to 10 mD in the deeper layers and 0.5 mD to 100 mD in the shallower layers. In the outfield, the permeability ranges from 0.1 mD to 1.5 mD in both the deep and shallow layers. This permeability structure is comparable generally with the Olkaria field in terms of the permeability range Ofwona (2002).

One key observation regarding the permeability structure of all versions of the model tested during this study is that in general the vertical permeability in the upflow tends to be quite low. In addition, the horizontal permeability is lower than expected in the deeper layers of the upflow zone. This is result of the inability of the standard AUTOUGH2 to simulate temperatures above 370°C. In order to maintain temperatures above 320 °C at 0 masl but below 370 °C only two model layers deeper, requires that low permeabilities are used. This is a key limitation of the current model and extending the model and its applicability using the super-critical version of AUTOUGH2 (Croucher & O'Sullivan, 2008) is an area of current research.

Note that some areas have a strongly anisotropic permeability (eg RHCCI) which represents a preferential flow direction, as indicated by the inflows and outflows in the downhole temperatures. This anisotropic permeability in the model rock-type corresponds to a preferential permeability in the real rock formation in the direction of the local faults.

Figure 11 shows that the best-calibrated model includes a low permeability structure separating the hotter part of the central upflow from the colder part. This coincides with the fault crossing the centre of the caldera inferred by Mibei and Lagat (2011). The low horizontal permeability of the fault could be attributed to fault gouge and to investigate the importance of the low-permeability structure another model was created with exactly the same permeability structure except that the low permeability was replaced with that of the neighbouring hotter central upflow zone.

Table 2: Permeability values of the best-fit model in the central upflow zone.

Rock Type	Model Permeability		
	k x mD	k y mD	k z mD
TSCCI	200	200	0.5
TSCHI	200	200	1
TUCCI	100	100	1
TUCHI	50	50	1
T0CCI	100	100	1
T0CHI	60	60	0.5
RHCCI	100	1	0.1
RHCHI	50	50	1
T1CCI	100	1	0.1
T1CHI	80	80	1
BACCI	40	40	0.5
BACHI	5	5	1
T2CCI	1	1	0.8
T2CHI	1.5	1.5	0.8

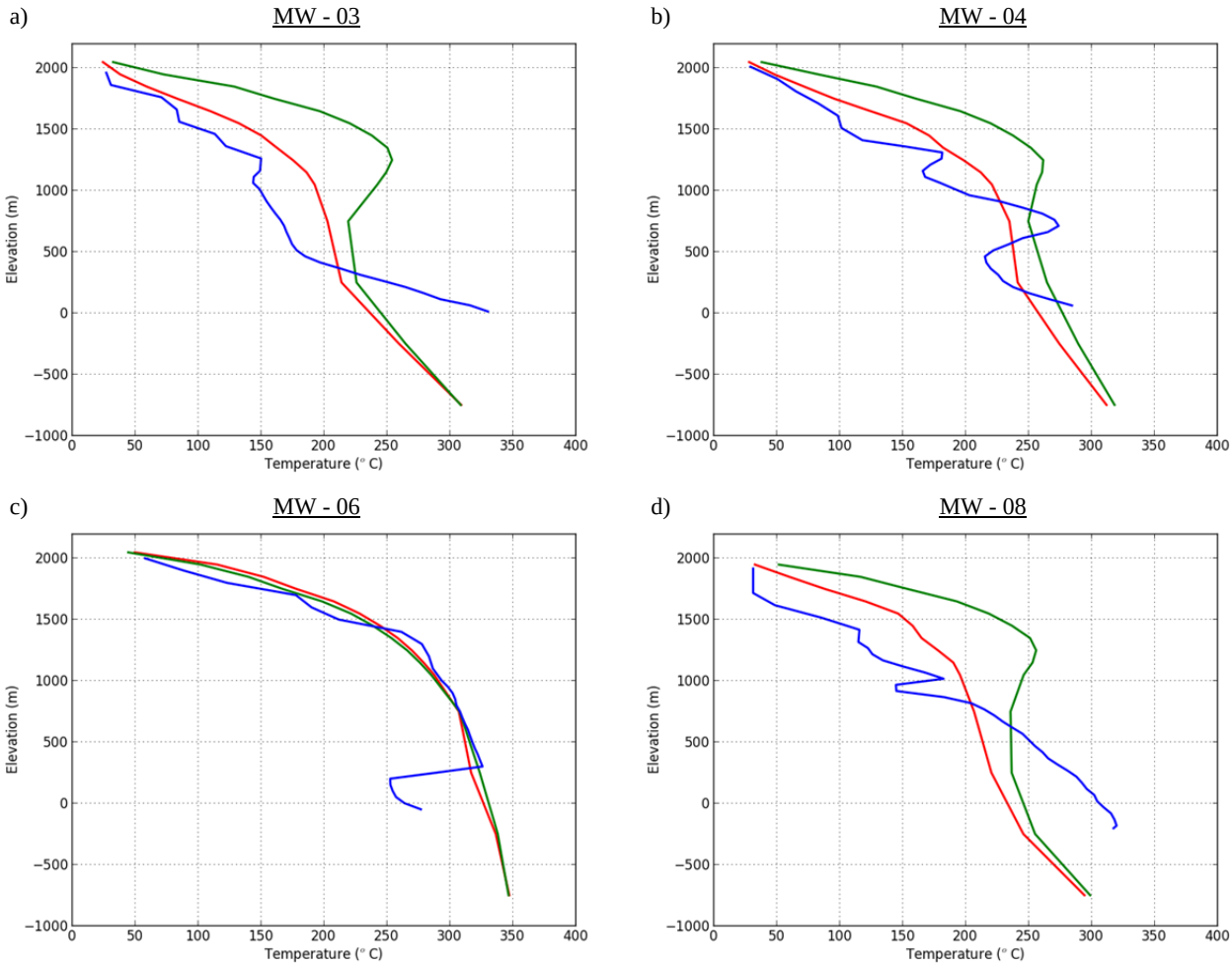

Figure 12: Downhole temperatures for four Menengai exploration wells. Measured data shown in blue, best-calibrated model results in red and model without low-permeability structure in green.

The results of this model are compared with the best-fit model and the field data in Figure 12. The model results for the downhole temperatures are largely unchanged for wells close to the centre of the upflow. Well MW-06 is shown in plot (c) is an example, while the others are not included. However, from plots (a), (b) and (d) it is clear that without the low-permeability structure the upflow plume spreads out to the northeast causing significantly greater than expected temperatures in the shallow layers. This provides a good example of the usefulness of the preliminary model in developing an understanding of the Menengai system.

Figure 13 shows the model temperatures along the cross-section B-B defined in Figure 2. The temperature contours agree well with those in the conceptual model section in Figure 4. The cold inflow from the right hand side at an elevation of 750 masl is captured, as is the offset of the plume to the left.

The plot of model gas saturation in Figure 14 shows both the unsaturated zone above the water table and that the model predicts the formation of a deeper steam zone. In the model this steam zone extends from 1600 masl down to 500 masl which agrees well with the alteration data discussed in Section 2.5. The model predicts a single steam zone rather than two distinct zones but is likely to be due to the vertical resolution of the model which is very coarse at these depths. In future models, a finer layer structure will be used which will allow the separation between the steam zones to be resolved.

5 PRODUCTION HISTORY MATCHING AND FUTURE SCENARIOS

Despite the very limited amount of production data, a qualitative production history matching exercise was carried out. For each of the four wells with data available the production feedzones were assigned and the best-fit natural state model was run using the mass flow production data (O'Sullivan *et al.*, 2001). The flowing enthalpies for all of the wells compared well with the measured values and so a number of qualitative future scenarios were also simulated. The plots in Figure 13 show the results for two of these scenarios.

Plot (a) shows the total steam flow taken from the system over 30 years of production for two different scenarios. The first scenario targets feedzones from 750 masl to 250 masl and the second targets feedzones from 250 masl to -250 masl. These elevations correspond to layers 14, 15 and 16 in the model. In both cases, the number of wells used and their wellhead locations were the same. The productivity of each well was estimated using the calibrated values of the existing wells and the schedule of connection dates was determined using realistic timeframes.

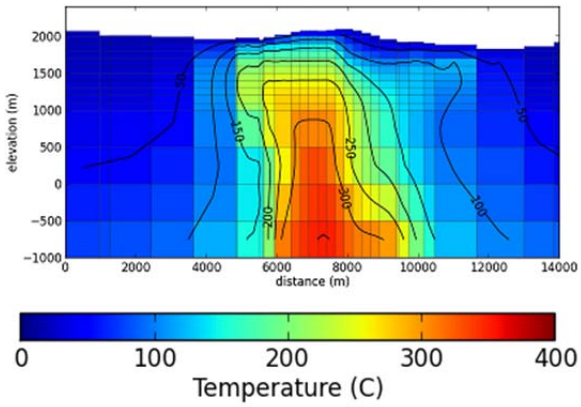

Figure 13: Model temperature (Section B-B in Figure 2).

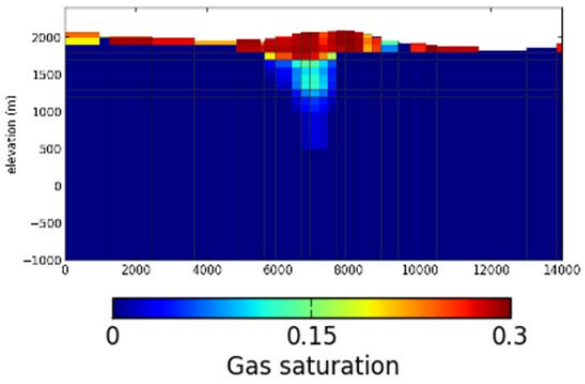

Figure 14: Model gas saturation (Section B-B in Figure 2).

a)

b)

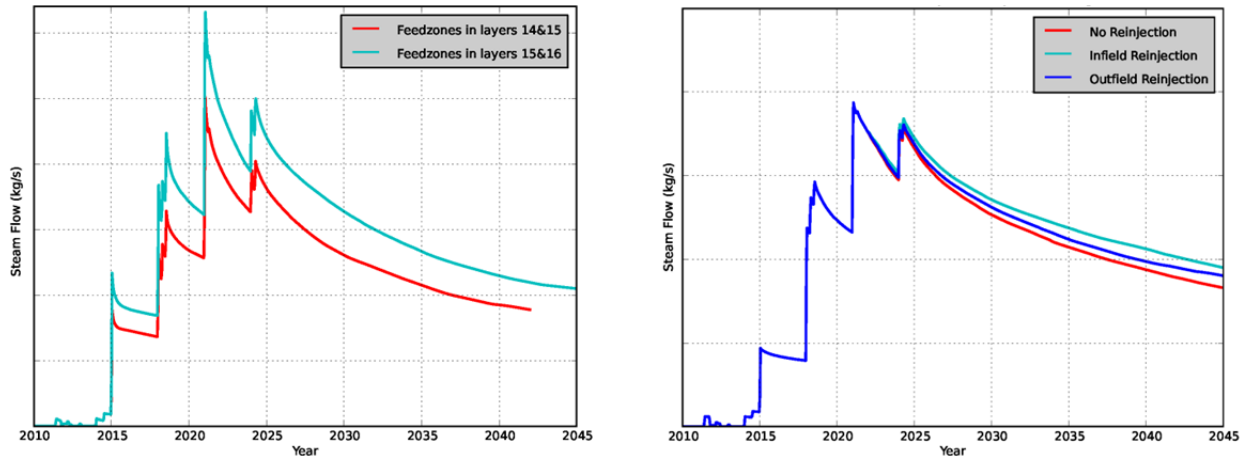

Figure 15: Qualitative results for future production scenarios using (a) different feedzone target depths and (b) different re-injection strategies.

The results confirm that the use of deeper feedzones achieves a higher steam production rate, despite the presence of the steam zone in layer 14 shown in Figure 14. This is because although the deeper fluid is in a liquid state, its higher temperature and pressure result in a higher total mass flow and higher total steam production.

The results of three scenarios using different re-injection strategies are shown in plot (b). In both cases, the deeper feedzone production scenario was used as the base case and again total steam production is shown. The re-injection was approximated by injecting warm water, with an enthalpy of 334.9 kJ/kg (corresponding to 80°C), into the appropriate model blocks. Re-injection was commenced in 2022, three years after production started, making a delayed re-injection strategy part of field development as suggested by Kaya and O'Sullivan (2010).

For the outfield re-injection case, locations were chosen by identifying the outfield blocks with higher permeability and also linked to the infield by permeable pathways (Kaya, 2010). For the infield re-injection locations were chosen with good permeability and close to zones that experience high-pressure decline. In both cases the amount re-injected was approximately 20% of the total mass flow and it was distributed across the re-injection blocks evenly. These preliminary results show that steam production rates for infield and outfield re-injection are both higher than for the no-reinjection case with the infield reinjection performing the best.

Worldwide experience has shown an optimum strategy involves a mix of infield and outfield re-injection. Infield re-injection provides pressure support to the main production zone, and reduces drawdown, but it may cause cold-water ingress, whereas outfield re-injection avoids the effect of thermal breakthrough (Kaya, 2010).

CONCLUSION

A conceptual model has been used to develop the first numerical model of the Menengai geothermal system. The numerical model was calibrated using the available downhole temperatures and has been found to produce a reasonable match to the field data. The model has also been used to investigate the possibility of a low-permeability structure running through the system and it was found that such a structure is likely to exist. Due to limitations of the standard AUTOUGH2 simulator, the model is unable to represent the deeper reservoir accurately and tends to underestimate the permeability in this region. Despite this problem, a number of qualitative production scenarios have been simulated, demonstrating the usefulness of a well-calibrated model. A new model capable of representing the super-critical region is currently under development.

ACKNOWLEDGEMENTS

The authors thank Cornel Ofwona for his valuable comments and inspiration to study the Menengai field. Thanks also go to the Geothermal Development Company for permission to publish the data and for their support.

REFERENCES

Croucher, A. E. & O'Sullivan, M. J. (2008), "Application of the computer code TOUGH2 to the simulation of supercritical conditions in geothermal systems," *Geothermics*, 37, 622-634.

Lagat, J. (2011), "Geothermal surface exploration approach: case study of Menengai geothermal field, Kenya," proceedings Kenya Geothermal Conference 2011, Kenyatta International Conference Centre Nairobi, November 21-21, 2011.

Lagat, J., Muturia, C., & Wanjie, C. (2010), "Menengai Prospect: Investigations for its Geothermal Potential," Internal Report, Geothermal Development Company.

Leat, P. T. (1984), "Geological Evolution of the Trachytic Caldera Volcano Menengai, Kenya rift Valley," *Journal of the Geological Society*, 141, 1057-1069. doi:10.1144/gsjgs.141.6.1057

Kaya, E. (2010), "Computer Modelling of Reinjection in Geothermal Fields," PhD Thesis, The University of Auckland.

Kaya, E., & O'Sullivan, M. (2010), "Modelling of Injection into Vapour-Dominated Geothermal systems," Paper presented at the World Geothermal Congress Bali, Indonesia.

Kipng'ok, J. (2011), "Fluid Chemistry, Feed Zones and Boiling in the First Geothermal Exploration Well at Menengai, Kenya," Report 15, Orkustofnun, Grensasvegur 9, IS-108 Reykjavik, Iceland: United Nations University.

McCall, G. J. H. (1967), "Geology of the Nakuru-Thomson's Falls lake Hannington Area," Ministry of Natural Resources Geological Survey of Kenya.

Mibei, G., & Lagat, J. (2011), "Structural Controls in Menengai Geothermal Field," proceedings Kenya Geothermal Conference 2011, Kenyatta International Conference Centre Nairobi, November 21-21, 2011.

Ofwona, C. O. (2002). A Reservoir Study of Olkaria East Geothermal System, Kenya. (Master of Science, University of Iceland). (1)

Omondi, C. (2011), "Borehole Geology and Hydrothermal Mineralisation of Wells MW-01 and MW-02, Menengai Geothermal Field, Central Kenya Rift Valley," Report 30, Orkustofnun, Grensasvegur 9, IS-108 Reykjavik, Iceland: United Nations university.

O'Sullivan, M. J., Pruess, K., & Lippmann, M. J. (2001), "State of the art of geothermal reservoir simulation," *Geothermics*, 30 (4), 395-429.

Pruess, K., Oldenburg, C., & Moridis, G. (1999), "TOUGH2 USER'S GUIDE, VERSION 2," Earth Sciences Division, Lawrence Berkeley National Laboratory: University of California.

Riaroh, D., & Okoth, W. (1994), "The Geothermal Fields of the Kenya Rift," *Tectonopyhsics*, 236, 117 - 130.

Simiyu, S. M. (2009), "Application of Micro-Seismic Methods to Geothermal Exploration: Examples from the Kenya Rift," *Short Course on Exploration for Geothermal Resources*: UNU-GTP, KenGen and GDC.

Simiyu, S. M., & Keller, G. R. (2001), "An Integrated Geophysical Analysis of the Upper Crust of the Southern Kenya Rift," *Geophysical Journal International*, 147, 543 - 561.

Suwai, J. J. (2011), "Preliminary Reservoir Analysis of Menengai Geothermal Field Exploration Wells," Report 32, Orkustofnun, Grensasvegur 9, IS-108 Reykjavik, Iceland: United Nations university.

Wheildon, J., Morgan, P., Williamson, K. H., Evans, T. R., & Swanberg, C. A. (1994), "Heat Flow in the Kenya Rift Zone," *Tectonopyhsics*, 236, 131-149.

Yeh, A., Croucher, A. & O'Sullivan, M.J. (2012), "Recent developments in the AUTOUGH2 simulator", Proceedings TOUGH Symposium 2012, Berkeley, California, September 17-19, 2012.